MICROBIOLOGY

Response thresholds in bacterial chemotaxis

Pushkar P. Lele,[1,2]* Abhishek Shrivastava,[2] Thibault Roland,[2] Howard C. Berg[2]

Stimulation of *Escherichia coli* by exponential ramps of chemoattractants generates step changes in the concentration of the response regulator, CheY-P. Because flagellar motors are ultrasensitive, this should change the fraction of time that motors spin clockwise, the CW_{bias}. However, early work failed to show changes in CW_{bias} when ramps were shallow. This was explained by a model for motor remodeling that predicted plateaus in plots of CW_{bias} versus [CheY-P]. We looked for these plateaus by examining distributions of CW_{bias} in populations of cells with different mean [CheY-P]. We did not find such plateaus. Hence, we repeated the work on shallow ramps and found that motors did indeed respond. These responses were quantitatively described by combining motor remodeling with ultrasensitivity in a model that exhibited high sensitivities over a wide dynamic range.

INTRODUCTION

Methylation and demethylation of bacterial chemotaxis receptors by CheR and CheB modulate receptor activity and enable precise restoration of response regulator output (*1*, *2*). Because binding of the response regulator, CheY-P, to FliM/FliN motor complexes modulates the probability of clockwise (CW) rotation, this enables perfect adaptation in flagellar motor output (CW_{bias}). Through the action of CheR and CheB, the chemotaxis network effectively computes time derivatives of a logarithm of the external ligand concentration (*3–6*). Hence, exponential ramps of chemoattractants administered to wild-type cells elicit a step change in [CheY-P] for the duration of the ramp (*7*). Because the receptor output remains constant during such ramps, they are particularly useful in quantifying the receptor output—motor response characteristics. In such experiments, Block *et al.* (*8*) observed thresholds in motor responses when the ramps were small ($<\pm 0.01$ s^{-1}); changes in CW_{bias} were only seen for ramps $>\pm 0.01$ s^{-1}. Because no corresponding thresholds to shallow ramps were observed in the levels of CheY-P monitored by a fluorescence resonance energy transfer technique (*7*), it appeared that flagellar motors filtered small changes in receptor output. Given that the motor is ultrasensitive to changes in [CheY-P] (*9*), how such filtering could be accomplished remained unclear.

CheR cheB mutants do not adapt, so CheY-P levels are directly set by the receptor activity (*10*). As a result, step changes in [CheY-P] can be produced in these mutants by applying step changes in attractants (*11*). Segall *et al.* subjected such mutants to step changes in a nonmetabolizable attractant α-methyl-D,L-aspartate and observed partial adaptation over a time scale of a few minutes. Yuan and co-workers showed that this partial adaptation results from addition to the motor of subunits of FliM (*12*). More recent work implicates FliN as well (*13*, *14*), so motor adaptation involves the remodeling of both FliM and FliN. On the basis of these observations, Tu and Berg (*15*) proposed a model that explained the thresholds in motor responses to shallow ramps. They assumed a nonlinear dependence of the number of FliM molecules, *N*, on CW_{bias} (Fig. 1A), which resulted in the nonsigmoidal relationship between bias and the concentration of CheY-P (Fig. 1B). Near the region indicated by the dashed lines in Fig. 1B, a small change in [CheY-P] due to slow ramps would result in imperceptible changes

in CW_{bias}, given the weak dependence on [CheY-P] near the plateau. However, a curve of this kind has not been observed experimentally (*9*).

Here, we designed a test of motor bias versus [CheY-P] by exploiting the heterogeneity in the distribution of CheY-P levels in cell populations. We did not observe a plateau in the relationship. Next, we subjected wild-type cells to slow exponential ramps (± 0.005 s^{-1}), observing partial adaptation in motor response but no thresholds. Finally, we built on a previous model to provide a molecular-level description of how differences in the strengths of binding of FliM/FliN in the motor enable partial adaptation to variations in [CheY-P]. Stochastic simulations of motor responses to step changes in [CheY-P] quantitatively reproduced our experimental results. Our data suggest an important role for remodeling in determining the long-term responses of the motor to ambient conditions.

RESULTS

Test of CW_{bias} versus [CheY-P] relationships

A heterogeneous distribution of CheY-P levels in a population of cells is expected to result in a range of CW_{bias} in the corresponding population of motors (*9*, *16*). Such heterogeneity in CheY-P levels arises due to stochastic noise associated with the output of the chemotaxis network (*17*, *18*). On the other hand, the adapted or steady-state CW_{bias} versus CheY-P relationship is an intrinsic property of the motor, and is independent of the chemotaxis network. Hence, the distribution of population CW_{bias} at a particular mean CheY-P level (μ_{CheY-P}) contains information regarding the spread of the CheY-P distribution (σ) and the CW_{bias} versus CheY-P relationship. For example, if the plateau shown in Fig. 1B indeed exists, then for a narrow distribution of CheY-P around the mean indicated by the dashed line, a significant fraction of the population of motors will have a bias similar to the one predicted by the plateau (CW_{bias} ~0.5). On the other hand, for a wide distribution of CheY-P, a significant fraction of the motors will have a CW_{bias} = 0 (or 1), with a smaller fraction exhibiting CW_{bias} ~0.5.

Measurements of CW_{bias} distributions

To test the nature of CW_{bias} versus [CheY-P], we measured CW_{bias} in populations of tethered *cheR cheB* cells. CheY was expressed from the genome under control of its native promoter. We set the mean level of CheY-P in each population via treatment with the nonmetabolizable

[1]Artie McFerrin Department of Chemical Engineering, Texas A&M University, College Station, TX 77843–3122, USA. [2]Department of Molecular and Cellular Biology, Harvard University, Cambridge, MA 02138, USA.
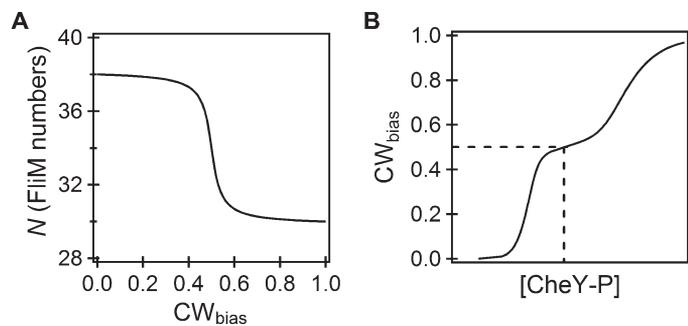*Corresponding author. E-mail: plele@tamu.edu

Fig. 1. Nonsigmoidal bias model. (A) Variation in FliM numbers as a function of CW_{bias}. **(B)** Resultant motor bias versus CheY-P levels. The dashed lines indicate CheY-P concentration at $CW_{bias} = 0.5$.

attractant α-methyl-D,L-aspartate (MeAsp), as outlined in our Materials and Methods section. Cell rotation was recorded via phase-contrast microscopy, and CW_{bias} was calculated over a minimum of 2 min. As seen in Fig. 2A, when treated with 0.1 mM MeAsp, a large fraction of the motors had a CW_{bias} ~1. When treated with 0.25 mM MeAsp (Fig. 2B), a sizeable fraction of the motors switched ($0 < CW_{bias} < 1$). Upon treatment with 0.35 mM MeAsp (Fig. 2C), most of the motors had a CW_{bias} ~0. Note that no peaks were discernible between $0 < CW_{bias} < 1$ in any of the experimental distributions. As we discuss below, such distributions are consistent with a model that excludes any plateaus in the relationship between CW_{bias} and [CheY-P]. A surprising observation was that in each experiment, CW-only and counterclockwise (CCW)–only motors were both seen, suggesting that the spread in [CheY-P] levels is considerable in *cheR cheB* strains.

Measurements of FliM numbers versus CW_{bias}

Because FliM/FliN remodeling undoubtedly plays a role in determining the CW_{bias} versus [CheY-P] relationship, we directly measured the FliM content in motors in individual tethered cells using methods described previously (*19*, *20*). In brief, single tethered cells of strains carrying *fliM-eyfp* on the genome were imaged via TIRF (total internal reflection fluorescence) microscopy and phase-contrast microscopy. CheY-P levels were controlled via an inducible plasmid (*cheY-pBAD34*). FliM numbers (N_S, where the subscript S indicates steady state) and CW_{bias} for each motor were calculated. These data ($n = 45$ motors) were combined with data sets previously collected [$n = 36$, Fig. 1C in Lele *et al.* (*19*)] to increase the sample size and enable more accurate estimations. The values for CW_{bias} were binned (bin size = 0.15), and the corresponding values of N_S were used to determine the average N_S for each bin. These averages were then divided by N_S^{CW} (the number of FliM molecules measured in CW-only motors) and plotted as a function of CW_{bias} in Fig. 2D. The data show a consistent decrease in these adapted N_S values with CW_{bias}.

Interpretation of CW_{bias} distributions

Early measurements at the level of single cells demonstrated that the relationship between steady-state motor bias and [CheY-P] could be very well fitted with a Hill curve (Hill coefficient ~10), indicating a steep, sigmoidal relationship (*9*). To distinguish between the sigmoidal and nonsigmoidal relationships for motor bias (Fig. 1), we predicted the distributions of CW_{bias} expected from either model in a population of cells containing a heterogeneous distribution of [CheY-P]. The distributions were calculated as a function of μ_{CheY-P} and σ in the
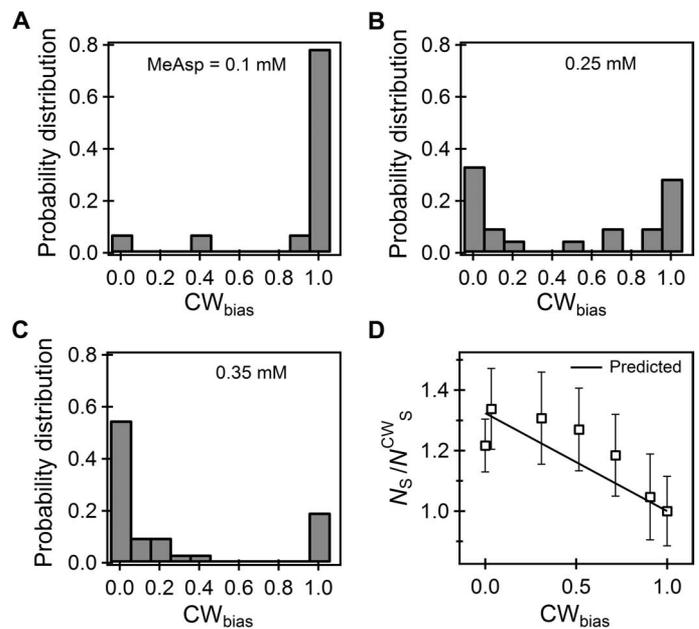

Fig. 2. Measurements of CW_{bias} and FliM numbers. (A to C) Measured distributions of motor bias in *cheR cheB* cells ($n = 17$ to 35). The concentration of attractant used for each experiment is indicated. **(D)** Experimentally determined number of FliM molecules in individual tethered motors versus CW_{bias}. Data were binned by CW_{bias} ($n = 81$ motors, bin size ~0.15), and the average N_S/N_S^{CW} is reported for each bin. Black curve represents predictions from Eq. 1, where N_S^{CCW}/N_S^{CW} ~1.32.

manner described in Appendix A. Qualitatively, the predictions from the sigmoidal model were consistent with experimental data over a range of values of μ_{CheY-P} and σ, given the absence of peaks in distributions between $0 < CW_{bias} < 1$. To quantitatively describe the data, we estimated the mean CheY-P levels and spread of CheY-P levels by fitting predictions to experimental density functions (Fig. 3A). The symbols are Gaussian kernel density estimates from the experimental data shown in Fig. 2 (A to C), and the shaded regions are probability densities for the predicted μ_{CheY-P}. We find that an SD for CheY-P of ~40 to 50% of the mean CheY-P level enabled the best fits to data as determined by χ^2 minimization. This suggests that the spread in CheY-P levels in *cheR cheB* strains ranges from ~1 to 2.5 μM.

Using a similar spread of CheY-P level (0.45 μ_{CheY-P}), we calculated the distributions from the nonsigmoidal model shown in Fig. 1B. These distributions are plotted in Fig. 3B. The Tu-Berg model assumed that the plateau is observed near a CW_{bias} ~0.5, because the original reports of thresholds in motor responses were observed near a prestimulus CW_{bias} ~0.5. As anticipated, the distributions predicted from the nonsigmoidal relationship indicate a peak around the plateau, CW_{bias} ~0.5. The absence of corresponding peaks in the experimental data suggests that the explanation for the observed thresholds is unlikely to be due to the model suggested by Tu and Berg (*15*). We note here that in the CW_{bias} versus [CheY-P] curves measured by Cluzel *et al.* (*9*), a small number of data points appeared to form a plateau near CW_{bias} ~0.15. Our analysis for motor bias distributions (Appendix A) predicts a sharp peak for such a plateau near CW_{bias} ~0.15, not seen in the data of Fig. 3. In any event, such a plateau, assuming it is not an artifact, is not relevant to the Tu-Berg model, because it cannot explain thresholds originally observed at CW_{bias} ~0.5.
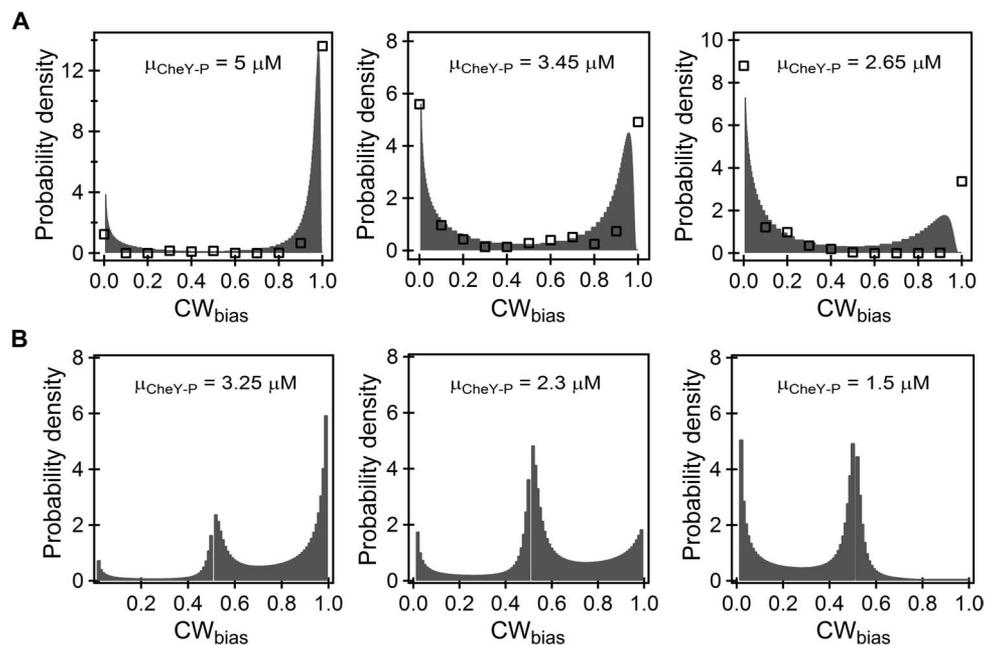
Fig. 3. Comparisons between nonsigmoidal and sigmoidal models. (**A**) Distributions of motor bias in a population of cells for decreasing mean values of [CheY-P] (left to right), computed from the data of Fig. 2 (A to C) (square symbols) or predicted (Appendix A) for a sigmoidal relationship between CW_{bias} and [CheY-P] (shaded). The mean value for each distribution is reported in the figure; $\sigma = 0.4$ to 0.5 μ_{CheY-P}. (**B**) Distributions of motor bias in a population of cells for decreasing mean values of CheY-P (left to right), predicted for the nonsigmoidal model shown in Fig. 1B. The mean value for each distribution is reported in the figure, $\sigma = 0.45$ μ_{CheY-P}.

Cell stimulation with exponential ramps

To determine conditions under which thresholds to exponential ramps of attractants might arise, we repeated the experiments of Block *et al.* (8) by subjecting wild-type cells to ramps of 0.005 s^{-1}, where thresholds were observed earlier for both up- and down-ramp. For these measurements, we used the protocols of Shimizu *et al.* (7), applied at room temperature. Tethered cells were subjected to repeated cycles of ramps: they were exposed to fixed concentrations of attractant for ~400 s, exposed to an exponential ramp in concentration either up or down for ~350 s, and then rapidly returned to the prestimulus level of attractant for another 400 s, before beginning the next ramp. The response of a motor to a single up-ramp is shown in Fig. 4A (top panel). As is evident, the CW_{bias} decreased immediately after the start of the ramp and recovered partially to a new CW_{bias} for the duration of the ramp. Because of the nonlinear relationship between CW_{bias} and CheY-P, any two cells undergoing an identical change in CheY-P level during a ramp will exhibit different changes in motor CW_{bias} depending on the prestimulus level of CheY-P. Hence, we selected motors that had similar prestimulus biases (~0.5) before averaging. The average of four such motors ($n = 4$, two replicates) is shown in Fig. 4A (middle panel).

The response of a motor to a single down-ramp is shown in Fig. 4B (top panel). As is evident, the CW_{bias} increased immediately after the start of the ramp and recovered partially to a new CW_{bias} for the duration of the ramp. The average of five motors ($n = 5$, each motor subjected to a single ramp cycle) with similar prestimulus CW_{bias} is shown in Fig. 4B (middle panel), with the corresponding attractant profile indicated in the bottom panel. As is evident, thresholds were not observed for either up- or down-ramp, in contrast to the previous report (8).
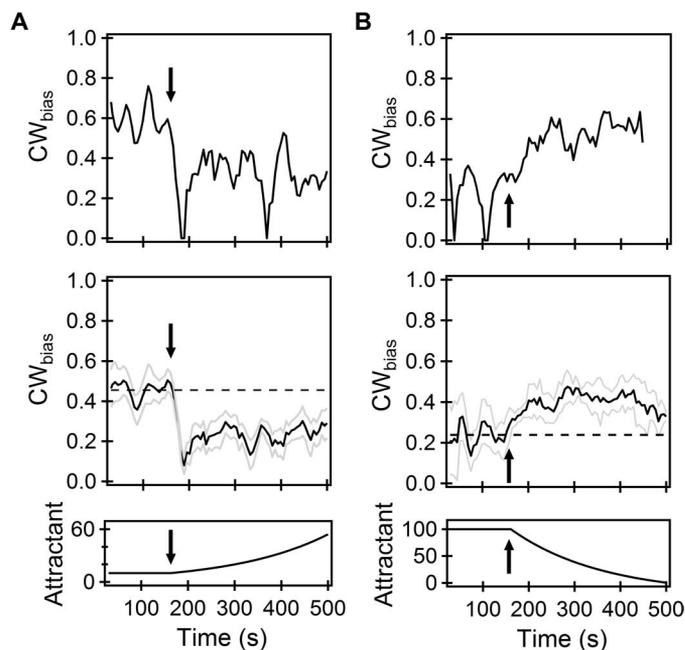

Fig. 4. Adaptation in wild-type cells subjected to exponential ramps of attractant. (**A**) Top panel: Response of a single motor to an up-ramp (0.005 s^{-1}). Middle panel: Average response of four motors each subjected to two ramp cycles. Bottom panel: Ramp profile. (**B**) Top panel: Response of a single motor to a down-ramp (−0.005 s^{-1}). Middle panel: Average response of five motors each subjected to a single ramp cycle. Bottom panel: Ramp profile. Dashed lines indicate prestimulus bias. Arrows indicate beginning of ramps. Faint gray lines indicate SD.

MODEL FOR RAMP RESPONSES

FliM/FliN remodeling as a function of bias

To predict the dependence of N_S on CW_{bias} shown in Fig. 2D, we modeled FliM/FliN dynamics based on a previous approach (19). We assumed that the total number of binding sites for FliM/FliN protomers (1 protomer = 1 FliM/4 FliN subunits) within the motor (M) remains the same irrespective of rotor conformation (CW or CCW). These sites are of two kinds: strong and weak. FliM/FliN protomers bound to weak sites continuously exchange with a pool of subunits in the cell even at steady state, consistent with experiments (19, 21, 22). Protomers bound to the strong sites are irreversibly attached [dissociation constant ~0 (19)], and these sites remain fully occupied with little or no exchange of FliM/FliN. The fraction of strong sites depends on motor conformation (M_{NE}^{CW}/M ~0.2 and M_{NE}^{CCW}/M ~0.6), where the subscript NE refers to nonexchanging and the superscript refers to the motor conformation. When a motor switches from CW to CCW, the fraction of strongly bound FliM/FliN protomers changes from ~0.2 to ~0.6. This variation drives stochastic fluctuations in the total number of FliM/FliN protomers, N, in a motor rotating with a constant CW_{bias}, as explained below.

Consider the case of a predominantly CW rotating motor with a steady-state number of FliM/FliN protomers (N_S). At $t = 0$ s, the motor switches to a CCW-only direction of rotation, resulting in an immediate increase in the number of strongly bound FliM. At this instant, among the previously attached N_S subunits, N_{NE}^{CCW} are now strongly bound causing a perturbation in the number of weakly bound protomers (see Appendix B). This perturbation forces the system to a new steady state: the process of binding and unbinding to the available weak sites continues, but the rate of binding is greater than the rate of unbinding (because there are very few weakly bound protomers after the switch). The imbalance in the rates of unbinding/binding drives an increase in N, with the increment limited by the amount of time the motor spends in the CCW conformation. If the motor rotates CCW indefinitely after the switch, a new steady-state value, N_S^{CCW}, will be reached. The time scales over which this remodeling occur are insensitive to CW_{bias} and agree very well with the observed time scales of remodeling ($1/k_{off}$ ~50 s) (12). The process is reversible. The entropic forces that drive the increase in FliM/FliN content when the motor switches from CW to CCW are also responsible for the decrease in FliM/FliN content when the motor switches from CCW to CW. The variation in N_S as a function of the CW_{bias} can be derived as (Appendix C)

$$N_S/N_S^{CW} = CW_{bias} + (1 - CW_{bias})N_S^{CCW}/N_S^{CW} \qquad (1)$$

The predictions from Eq. 1 are shown in Fig. 2D (black curve), consistent with the observed trend in experimental data.

Model for ultrasensitivity

CheY-P is predicted to bind with a higher affinity to the FliM/FliN complex in the CW conformation than in the CCW conformation, characterized by two dissociation constants K_{CW} and K_{CCW}, with K_{CCW} ~4 K_{CW} (23, 24). The number of CheY-P bound to the motor at any instant is governed by the ligand concentration and the number of FliM/FliN protomers within the motor. We calculated the number of CheY-P bound to the motor (Y_B) using simple first-order binding relations

$$Y_B = (1 - CW_{bias})\frac{c}{c + K_{CCW}}N_S^{CCW} + CW_{bias}\frac{c}{c + K_{CW}}N_S^{CW} \qquad (2)$$

where c is the CheY-P concentration, and N_S^{CCW} and N_S^{CW} refer to the number of FliM/FliN protomers in the two states. The first term in Eq. 2 accounts for binding to the motor when it rotates CCW, and the second accounts for binding to the motor when it rotates CW.

On the basis of a previous model (25), we assume that the number of CheY-P bound to the motor determines the offset to the free-energy difference in the CW and CCW states of the FliG ring. We assume that the FliG ring contains a fixed number of subunits (N_{FliG}), independent of the direction of motor rotation (26, 27). When a very low number of CheY-P is bound, the CCW state is energetically more favorable and the motors have a lower probability of rotating CW. Each CheY-P molecule bound reduces the free-energy difference by a constant energy offset, Ψ, and the probability of CW rotation is calculated using a two-state model

$$CW_{bias} = \frac{1}{1 + \exp(N_{FliG}E - \Psi Y_B)} \qquad (3)$$

Here, E refers to the free-energy difference between the CCW and CW states of the FliG ring (Fig. 5A) in the absence of [CheY-P]. Fitting Eq. 3 using an iterative χ^2 minimization (Levenberg-Marquardt algorithm) to previous data for steady-state motor bias versus [CheY-P] (9) yielded three parameters: $K_{CW} = 2.61 \pm 1.02$, $E = 0.22 \pm 0.02$ k_BT, and $\Psi = 0.35 \pm 0.01$ k_BT. Residuals calculated using Eq. 3 were smaller (sum of residuals = 0.28) than calculated using the Hill equation (sum of residuals = 0.32). Thus, our model fits previous data better than the Hill function, which is expected considering that we use three fitting parameters compared to two in the Hill function (K_D and h). The measurements by Cluzel et al. (9) represent adapted motor responses after remodeling (12, 28), and hence, these fitted values reflect the steady-state motor behavior. Here, we make a very reasonable assumption that the values of Ψ, E, and K_{CW} remain constant irrespective of the variations in [CheY-P] or N, which enable us to use these values to predict transient motor responses observed during ramps.

Remodeling occurs on a slower time scale compared to the time scales over which motors respond to changes in [CheY-P]. Therefore, the instantaneous motor sensitivity is in fact determined by the number of FliM/FliN subunits already present in the motor at that instant. Remodeling of FliM/FliN shifts the instantaneous motor response versus [CheY-P] curve, similar to the methylation/demethylation-mediated shifts in kinase activity versus ligand curves. The true sensitivity of the motor, which determines its short-term response to fluctuations in [CheY-P], has been recently measured for fixed values of FliM/FliN (28). For the values we obtained by fitting Eq. 3, we predict responses for fixed values of FliM/FliN (that is, transient motor responses) comparable with those reported by Yuan and Berg (28) (see fig. S1). Finally, because Eq. 2 calculates the increase or decrease in the number of CheY-P bound to the motor as a result of remodeling, it connects remodeling with the ultrasensitivity of the switch.

Stochastic simulations of motor responses to exponential ramps

To test if our model could quantitatively explain the role of FliM/FliN remodeling in motor responses in wild-type cells subjected to exponential ramps, we carried out stochastic simulations of motor dynamics, as discussed here. The model equations and algorithms are detailed in Appendix B and in the Supplementary Materials. Briefly, the simulations are initialized at $t = -80$ s, with a motor at an initial CW_{bias}

and containing N_S protomers (as determined by Eq. 1). Motor switching traces (fig. S2) were then generated for the initial CW_{bias} by sampling wait times for CCW (τ_{CCW}) and CW rotations (τ_{CW}) from exponential distributions of respective intervals. The mean values of these distributions have been experimentally determined to vary with CW_{bias} (24), as shown in fig. S3. Each time a switch occurs, the number of strongly bound FliM/FliN changes to one of the only two possible values (N_{NE}^i). This perturbs the number of weakly bound protomers, leading to a fluctuation in the number of protomers even under steady-state conditions (no attractants added). These stochastic fluctuations in each interval (CCW or CW) were modeled via a simple Monte-Carlo scheme (29) using the equations in Appendix B and the parameters in Table 1. For very short intervals, often no fluctuations occurred because FliM/FliN exchange occurs on relatively slower time scales. For longer intervals, subunits attached more often (compared to detachment) when the motor rotated CCW, and detached more often (compared to attachment) when the motor rotated CW. We assumed that Y_B varied instantaneously with each FliM/FliN addition or removal, according to Eq. 2 (see the Supplementary Materials). The probability of CW rotation was updated via Eq. 3 each time a fluctuation in Y_B occurred, which resulted in a change in the mean interval times for both CW and CCW rotation, according to the experimental measurements shown in fig. S3. The simulations were then repeated by sampling from exponential wait time distributions with the updated means. The time-varying CW_{bias} was calculated from such motor switching traces with a 20-s moving-average window (12).

We focused on the up-ramp experiments, shown in Fig. 4A. At time $t \sim -35$ s, the CheY-P level was changed to a lower value and held constant, representing a wild-type cell subjected to exponential ramps in attractant level. The change in CheY-P level generated a drop in the probability of CW rotation, calculated from Eqs. 2 and 3. This change in CheY-P level (ΔCheY-P) was used as a free parameter to ensure that the drop in the predicted CW_{bias} matched the dip in the experimental curve. The motor now predominantly rotated CCW. As discussed previously, the numbers of FliM/FliN protomers in the motor grow because the motor spends more time in the CCW conformation. Upon each addition of a subunit, the probabilities of CW rotation were recalculated and the means of the sampling distributions were updated. The process was run in a loop (~250 iterations). The average of simulated traces of N versus time (Fig. 5B) and the corresponding time variations in CW_{bias} (Fig. 5C) are shown by the solid black curve ($n = 11$ motors). Next, for the same value of ΔCheY-P, we repeated the simulations for a case in which the FliM/FliN complex does not remodel (gray curve in Fig. 5C). The open symbols indicate experimental data from Fig. 4A (middle panel). The simulated results (with FliM/FliN remodeling) are in close agreement with experimental observations, whereas predictions without FliM/FliN remodeling fail to capture observed trends. Similarly, simulation results for the down-ramp are also in agreement with the experiments (see the Supplementary Materials).
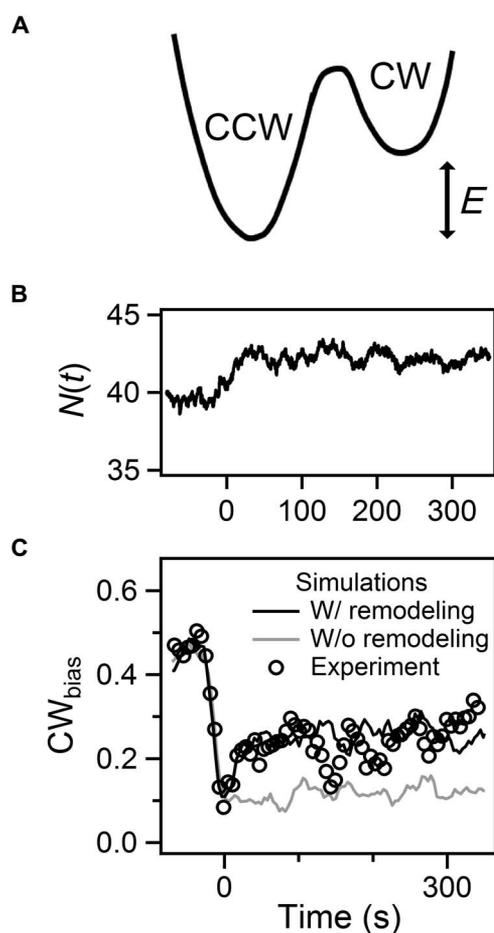
DISCUSSION

Our measurements of single-motor responses to exponential ramps in attractants failed to show the thresholds previously observed by Block et al. (8). Block et al. subjected the same cells to repeated cycles of up- and down-ramp over periods of an hour or more. The thresholds

Fig. 5. Stochastic simulations of motor responses to ramps. (**A**) Two-state model for motor switching. In the absence of a ligand, the free-energy difference in the two states of the motor is E, and the CCW conformation is favored. (**B**) Average of simulated traces for motor adaptation in wild-type cells to exponential ramps ($n = 11$ motors). Reduction in CheY-P levels due to an exponential ramp in attractant level before $t = 0$ s causes an increase in $N(t)$, the FliM/FliN content. (**C**) This results in a corresponding increase in CW_{bias}. The solid black curve represents simulations with FliM/FliN remodeling. The solid gray curve represents simulations without FliM/FliN remodeling. The open circles indicate experimental measurements from Fig. 4A (middle panel).

Table 1. Parameters used in the study.

Parameter	Values
$k_{off} = k_{on}$ (for CW and CCW)	~0.02 s^{-1} [Lele et al. (19)]
M	56 [Lele et al. (19)]
N_S^{CW}	34 (Thomas et al., 2006)
N_{NE}^{CW}, N_{NE}^{CCW}	12, 34 [Lele et al. (19)]
E	0.22 k_BT (this work)
Ψ	0.35 k_BT (this work)
K_{CW}	2.61 (this work)

that appeared in those experiments at the ramp rates used here ($0.005\ \mathrm{s}^{-1}$) might have been due to desensitization of receptor adaptation owing to exhaustion of intermediates not replenished by growth, a problem that might be revealed by measurements of [CheY-P]. Our analysis, on the other hand, was conducted on data sets no more than 25 min long.

The addition/removal of FliM/FliN subunits and the consequent shifts in motor response curves appear similar in principle to the effect of methylation/demethylation on kinase activity. This raised the possibility that motor remodeling plays an analogous role by enabling precise adaptation at the motor level, an ability that would be manifest in the form of a plateau in CW_{bias} versus [CheY-P] relationship. However, our measurements of motor dynamics as well as adapted motor response curves rule out such a possibility. Instead, remodeling enhances motor sensitivity. For a fixed number of FliM/FliN protomers, the CW_{bias} versus [CheY-P] relationship is relatively steep [Hill coefficient ~20; (28)]. This sensitivity controls short-term responses of the motor to even weak signals: a small drop in [CheY-P] results in a transient rise in CCW bias, enabling the cell to move up the gradient of attractants. To retain this sensitivity over a wide range of signal levels, the motor must remodel the switch to shift its operating point, albeit gradually, given the slow kinetics of FliM/FliN assembly. This can be quantitatively described in terms of a mechanistic model that posits that a difference in the number of strong binding sites for FliM/FliN in the two rotor conformations drives motor remodeling (19). This model is consistent with the experimentally observed steady-state rates of FliM/FliN exchange, the independence of these rates on motor conformations, and the presence of a motor-bound fraction of FliM/FliN that does not exchange, conditions not met by previous approaches to motor remodeling (15, 30). Stochastic simulations, based on a model that combines remodeling and ultrasensitivity, are able to quantitatively predict motor responses to shallow ramps, confirming the role of motor remodeling in determining the long-term motor response (CW_{bias}) to ambient conditions. Thus, remodeling complements the short-term memory due to receptor methylation, while also acting as a fail-safe to protect against inherent heterogeneities in the output of the chemotaxis network.

MATERIALS AND METHODS

Strains and plasmids
Strain HCB1697—$\Delta cheB$, $\Delta cheY$, $\Delta cheZ$, $\Delta flgE$, $fliM$-$eyfp$(A206K), with p$Trc99A$-$flgE$ and p$BAD34$-$cheY$—was used for TIRF measurements. Strain JY35—$\Delta cheR$ $\Delta cheB$, carrying the sticky $fliC$ allele on a chloramphenicol-resistant plasmid (pKAF131)—was used for population activity measurements. Strains were grown in tryptone broth at 33°C to OD_{600} (optical density at 600 nm) = 0.5, and ampicillin (100 μg/liter) and chloramphenicol (5 μg/ml) were added depending on the strain. Protein expression was induced with IPTG (isopropyl-β-D-thiogalactopyranoside) (0 to 50 μM) and arabinose (0 to 0.01%) when necessary. Cells were washed twice with motility buffer [0.01 M potassium phosphate (pH 7.0), 10^{-4} M EDTA, 0.067 M NaCl, 0.01 M sodium lactate, and 10^{-6} M L-methionine].

Population activity measurements
After washing cells two times in motility buffer, the flagella were sheared and separated from the cells via centrifugation. The pelleted cells were resuspended in attractants of desired concentrations for 5 to 10 min. The cells were then tethered in tunnel slides, and cell rotation was recorded using a digital camera (Thorlabs DCC1240M) at 67 fps. Rotational speeds

and switching statistics were determined using custom-written codes in MATLAB.

Single-cell responses to ramps
In addition to selecting cells with a similar CW_{bias}, we ignored cells that either stopped rotation before the completion of the experiment or exhibited long pauses, because it was not possible to track the CW_{bias} in these cases. A large fraction of tethered cells were observed to detach from the coverslip over the long duration (400 to 500 s) of a typical ramp experiment, which significantly reduced the size of our data. The cells included in calculations of the averages shown in Fig. 4 conformed to these criteria.

APPENDIX A

Predicting distributions
Let B and C represent random variables describing CW_{bias} and CheY-P level. C is assumed to be normally distributed and B here is a monotonically increasing function of C, $B = g(C)$, which can be uniquely solved for C such that $C = \phi(B)$. The probability density for B is calculated as

$$h(B) = f(\phi)\frac{d\phi}{dB} \tag{A1}$$

The relationship between CW_{bias} and CheY-P concentrations (c), predicted by an MWC-type relationship (15), is given by

$$CW_{bias} = g(c)$$
$$= \frac{L(1 + c/K_{CW})^{N_S}}{L(1 + c/K_{CW})^{N_S} + (1 + c/K_{CCW})^{N_S}} \tag{A2}$$

where the equilibrium constant for transitions between the CW and CCW states is L (in the absence of the ligand). Setting N_S as the nonlinear function shown in Fig. 1A [Eq. 7 in Tu and Berg (15)] yields the motor response shown in Fig. 1B. Solving for c yields

$$c = \phi(CW_{bias})$$
$$= \frac{K_{CCW} - K_{CW}}{\frac{K_{CCW}}{K_{CW}}\exp\left(\frac{1}{N}\ln\left[L\frac{1 - CW_{bias}}{CW_{bias}}\right]\right) - 1} - K_{CW}. \tag{A3}$$

$\phi(CW_{bias})$ is differentiable over all positive values of CheY-P (except at CheY-P = CheY-$P_{CW_{bias}=0.5}$). Solving for $h(B)$ enables predictions of the probability densities expected from the nonsigmoidal model (Fig. 3B). A similar approach is used to predict the distributions expected from a sigmoidal model (Fig. 3A).

APPENDIX B

Remodeling motors
The total available sites (M) for FliM/FliN protomers are assumed to remain constant irrespective of motor conformation. M consists of two types of sites—the strong sites, which are fully occupied by subunits at all times, N_{NE}^i, and the weak sites, some of which are occupied (C) and some that are vacant (B). The superscript $i \in$ CW, CCW indicates that N_{NE}^i can take on one of two possible values in a given interval, depending on the motor conformation. At steady state (constant CW_{bias}),

the motor consists of a steady number of protomers (N_S), and M, B, C, and N_{NE} are related as

$$M = N_{NE}{}^i + C_S + B_S \qquad (B1)$$

The total protomers in the motor are

$$N = N_{NE}{}^i + C_S \qquad (B2)$$

Whenever a switch in conformation occurs (say at $t = 0$ s), N_{NE} assumes a new value, $N_{NE}{}^j$ ($j \neq i$), thereby perturbing C_S. This perturbation is expressed as

$$C(0) = N(0) - N_{NE}{}^j \qquad (B3)$$

where $N(0)$ refers to the total FliM/FliN protomers existing in the motor at the instant of the switch in motor conformation. The system evolves to a new steady state after the perturbation. This evolution is governed by the dynamics of the weakly bound protomers and is limited by the amount of time that the motor spends in the new conformation. The kinetics driving the relaxation are

$$\frac{dC}{dt} = k_{on}B - k_{off}C \qquad (B4)$$

and at steady state

$$B_S = \frac{k_{off}}{k_{on}} C_S \qquad (B5)$$

Here, k_{on} is the pseudo–first-order on-rate and k_{off} is the off-rate for FliM subunits attached to weak sites.

APPENDIX C

Deriving N_S versus CW_{bias}

Consider a motor that switches between the two directions of rotation with a constant CW_{bias}. Let the mean wait times for the CW and CCW events be represented by λ_{CW}, λ_{CCW} ($\ll 1/k_{off}$). The number of FliM/FliN protomers will fluctuate around a time-averaged value N_0 due to the switches between CW and CCW. Starting with $N_S = N_0$ at the instant when the motor switches to the CCW conformation ($t = t_0$) for τ seconds, the positive fluctuation or the number of FliM/FliN protomers added over that interval can be calculated from Eqs. B1 to B5 in Appendix B. Solving the equations yields the relation for the added subunits

$$\Delta N^{CCW} = (N_S^{CCW} - N_0)(1 - e^{-(k_{off} + k_{on})\tau}) \qquad (C1)$$

First, consider only the positive fluctuations (each time a motor switches to CCW). The probability density function (pdf) for ΔN^{CCW} can be calculated from the pdf for τ, which is exponentially distributed with a mean wait time of λ_{CCW}. The expression for the pdf of ΔN^{CCW} is

$$f(\Delta N^{CCW}) = \frac{\lambda_{CCW}}{(k_{off} + k_{on})(N_S^{CCW} - N_0)} \left(\frac{\Delta N^{CCW}}{N_0 - N_S^{CCW}} + 1 \right)^{\frac{\lambda_{CCW}}{(k_{off} + k_{on})} - 1} \qquad (C2)$$

Similarly, the pdf for negative fluctuations (each time the motor switches to CW) is

$$f(\Delta N^{CW}) = \frac{\lambda_{CW}}{(k_{off} + k_{on})(N_S^{CW} - N_0)} \left(\frac{\Delta N^{CW}}{N_0 - N_S^{CW}} + 1 \right)^{\frac{\lambda_{CW}}{(k_{off} + k_{on})} - 1} \qquad (C3)$$

The positive and negative fluctuations cancel each other over time, such that on an average $N_S = N_0$. That is, the means of the two fluctuations are equal and opposite in sign, which enables determination of the relationship between N_S and CW_{bias}

$$\overline{\Delta N^{CCW}} + \overline{\Delta N^{CW}} = 0$$

$$\therefore \int_0^{N_S^{CCW} - N_0} \Delta N^{CCW} f(\Delta N^{CCW}).d\Delta N^{CCW} + \int_0^{N_S^{CW} - N_0} \Delta N^{CW} f(\Delta N^{CW}).d\Delta N^{CW} = 0 \qquad (C4)$$

Integrating the above equation and algebraically manipulating the resulting expression yield Eq. 1 shown in the main text.

SUPPLEMENTARY MATERIALS

Supplementary material for this article is available at http://advances.sciencemag.org/cgi/content/full/1/9/e1500199/DC1
Fig. S1. CW_{bias} versus CheY-P for fixed values of N (gray dotted and solid curves).
Fig. S2. Motor switching trace simulated by alternately sampling exponential distributions of CW and CCW wait-time intervals.
Fig. S3. Variations in mean intervals with CW_{bias}.
Fig. S4. Comparisons between experimental and simulation results for a down-ramp (-0.005 s^{-1}).

REFERENCES AND NOTES

1. N. Barkai, S. Leibler, Robustness in simple biochemical networks. *Nature* **387**, 913–917 (1997).
2. U. Alon, L. Camarena, M. G. Surette, B. Aguera y Arcas, Y. Liu, S. Leibler, J. B. Stock, Response regulator output in bacterial chemotaxis. *EMBO J.* **17**, 4238–4248 (1998).
3. F. W. Dahlquist, P. Lovely, D. E. Koshland Jr., Quantitative analysis of bacterial migration in chemotaxis. *Nat. New Biol.* **236**, 120–123 (1972).
4. Y. V. Kalinin, L. Jiang, Y. Tu, M. Wu, Logarithmic sensing in *Escherichia coli* bacterial chemotaxis. *Biophys. J.* **96**, 2439–2448 (2009).
5. D. A. Brown, H. C. Berg, Temporal stimulation of chemotaxis in *Escherichia coli*. *Proc. Natl. Acad. Sci. U.S.A.* **71**, 1388–1392 (1974).
6. Y. Tu, Quantitative modeling of bacterial chemotaxis: Signal amplification and accurate adaptation. *Annu. Rev. Biophys.* **42**, 337–359 (2013).
7. T. S. Shimizu, Y. Tu, H. C. Berg, A modular gradient-sensing network for chemotaxis in *Escherichia coli* revealed by responses to time-varying stimuli. *Mol. Syst. Biol.* **6**, 382 (2010).
8. S. M. Block, J. E. Segall, H. C. Berg, Adaptation kinetics in bacterial chemotaxis. *J. Bacteriol.* **154**, 312–323 (1983).
9. P. Cluzel, M. Surette, S. Leibler, An ultrasensitive bacterial motor revealed by monitoring signaling proteins in single cells. *Science* **287**, 1652–1655 (2000).
10. V. Sourjik, H. C. Berg, Receptor sensitivity in bacterial chemotaxis. *Proc. Natl. Acad. Sci. U.S.A.* **99**, 123–127 (2002).
11. J. E. Segall, S. M. Block, H. C. Berg, Temporal comparisons in bacterial chemotaxis. *Proc. Natl. Acad. Sci. U.S.A.* **83**, 8987–8991 (1986).
12. J. Yuan, R. W. Branch, B. G. Hosu, H. C. Berg, Adaptation at the output of the chemotaxis signalling pathway. *Nature* **484**, 233–236 (2012).
13. R. W. Branch, M. N. Sayegh, C. Shen, V. S. J. Nathan, H. C. Berg, Adaptive remodelling by FliN in the bacterial rotary motor. *J. Mol. Biol.* **426**, 3314–3324 (2014).
14. N. J. Delalez, R. M. Berry, J. P. Armitage, Stoichiometry and turnover of the bacterial flagellar switch protein FliN. *mBio* **5**, e01216-14 (2014).
15. Y. Tu, H. C. Berg, Tandem adaptation with a common design in *Escherichia coli* chemotaxis. *J. Mol. Biol.* **423**, 782–788 (2012).
16. F. Bai, Y.-S. Che, N. Kami-ike, Q. Ma, T. Minamino, Y. Sowa, K. Namba, Populational heterogeneity vs. temporal fluctuation in *Escherichia coli* flagellar motor switching. *Biophys. J.* **105**, 2123–2129 (2013).
17. M. D. Levin, C. J. Morton-Firth, W. N. Abouhamad, R. B. Bourret, D. Bray, Origins of individual swimming behavior in bacteria. *Biophys. J.* **74**, 175–181 (1998).
18. M. Kollmann, L. Løvdok, K. Bartholomé, J. Timmer, V. Sourjik, Design principles of a bacterial signalling network. *Nature* **438**, 504–507 (2005).

19. P. P. Lele, R. W. Branch, V. S. Nathan, H. C. Berg, Mechanism for adaptive remodeling of the bacterial flagellar switch. *Proc. Natl. Acad. Sci. U.S.A.* **109**, 20018–20022 (2012).

20. P. P. Lele, B. G. Hosu, H. C. Berg, Dynamics of mechanosensing in the bacterial flagellar motor. *Proc. Natl. Acad. Sci. U.S.A.* **110**, 11839–11844 (2013).

21. H. Fukuoka, Y. Inoue, S. Terasawa, H. Takahashi, A. Ishijima, Exchange of rotor components in functioning bacterial flagellar motor. *Biochem. Biophys. Res. Commun.* **394**, 130–135 (2010).

22. N. J. Delalez, G. H. Wadhams, G. Rosser, Q. Xue, M. T. Brown, I. M. Dobbie, R. M. Berry, M. C. Leake, J. P. Armitage, Signal-dependent turnover of the bacterial flagellar switch protein FliM. *Proc. Natl. Acad. Sci. U.S.A.* **107**, 11347–11351 (2010).

23. T. A. J. Duke, N. Le Novère, D. Bray, Conformational spread in a ring of proteins: A stochastic approach to allostery. *J. Mol. Biol.* **308**, 541–553 (2001).

24. F. Bai, R. W. Branch, D. V. Nicolau Jr., T. Pilizota, B. C. Steel, P. K. Maini, R. M. Berry, Conformational spread as a mechanism for cooperativity in the bacterial flagellar switch. *Science* **327**, 685–689 (2010).

25. L. Turner, A. D. T. Samuel, A. S. Stern, H. C. Berg, Temperature dependence of switching of the bacterial flagellar motor by the protein CheY^{13DK106YW}. *Biophys. J.* **77**, 597–603 (1999).

26. Y. Sowa, A. D. Rowe, M. C. Leake, T. Yakushi, M. Homma, A. Ishijima, R. M. Berry, Direct observation of steps in rotation of the bacterial flagellar motor. *Nature* **437**, 916–919 (2005).

27. S. Nakamura, N. Kami-ike, J.-. P. Yokota, T. Minamino, K. Namba, Evidence for symmetry in the elementary process of bidirectional torque generation by the bacterial flagellar motor. *Proc. Natl. Acad. Sci. U.S.A.* **107**, 17616–17620 (2010).

28. J. Yuan, H. C. Berg, Ultrasensitivity of an adaptive bacterial motor. *J. Mol. Biol.* **425**, 1760–1764 (2013).

29. X. Cai, Exact stochastic simulation of coupled chemical reactions with delays. *J. Chem. Phys.* **126**, 124108 (2007).

30. Y. S. Dufour, X. Fu, L. Hernandez-Nunez, T. Emonet, Limits of feedback control in bacterial chemotaxis. *PLOS Comput. Biol.* **10**, e1003694 (2014).

Lele *et al. Sci. Adv.* 2015;1:e1500299   16 October 2015

8 of 8

Response thresholds in bacterial chemotaxis

Pushkar P. Lele, Abhishek Shrivastava, Thibault Roland and Howard C. Berg

ARTICLE TOOLS	http://advances.sciencemag.org/content/1/9/e1500299
SUPPLEMENTARY MATERIALS	http://advances.sciencemag.org/content/suppl/2015/10/13/1.9.e1500299.DC1
REFERENCES	This article cites 30 articles, 12 of which you can access for free http://advances.sciencemag.org/content/1/9/e1500299#BIBL
PERMISSIONS	http://www.sciencemag.org/help/reprints-and-permissions

Use of this article is subject to the Terms of Service